Continuous Rapid-Beam-Scanning and Circular-Polarized Leaky-Wave Antenna Based on Meandering-SIW with Defected Ground Structures

RUAN Yizheng, NIU Zhenyi, CHEN Weikang, ZHAO Yongjiu, PAN Shilong*

National Key Laboratory of Microwave Photonics, Nanjing University of Aeronautics and Astronautics, Nanjing 211106, P. R. China

(Received 26 September 2024; revised 12 January 2025; accepted 16 February 2025)

Abstract: A compact high-scanning-rate circular-polarized leaky-wave antenna (LWA) based on a meandering substrate integrated waveguide (SIW) with defected ground structures (DGSs) is presented. The meandering-SIW design is employed to enhance the beam scanning rate, while circular polarization is achieved by etching π-shaped slots on the top plane. To suppress the open stopband at broadside, offset circular DGSs are periodically etched on the ground plane. Their impact on the reflection coefficient and axial ratio is then analyzed through a parametric study. A prototype of the antenna is simulated, fabricated, and measured. Both simulated and measured results indicate a scanning rate of approximately 8.6, with continuous beam scanning from −41° to 59° across the 11.3—12.7 GHz operating band. The antenna maintains an axial ratio below 3 dB within the 11.5—12.3 GHz range. This design shows promise for use in wireless communication systems, particularly in environments with increasingly limited spectrum resources.

Key words: leaky-wave antenna (LWA); scanning rate; circular polarization; open stopband; defected ground structure (DGS)

CLC number: TN825 **Document code:** A **Article ID:** 1005-1120(2025)01-0080-10

0 Introduction

Leaky-wave antennas (LWAs) have garnered considerable attention in recent years, particularly in wireless communication and microwave applications. This interest is largely due to their ability to scan beams with frequency and their simple feeding networks[1-2]. A key performance factor for LWAs is their scanning range, which is critical in many applications. However, achieving wide-angle beam scanning typically demands significant spectrum resources[3-4]. This poses challenges for certain applications, as the antenna's excitation requires a broader bandwidth, which can be difficult to implement in practice.

Recently, several methods have been proposed to enhance the scanning rate of linearly polarized (LP) antennas, including slow-group-delay transmission lines[5-6], composite right/left-handed (CRLH) transmission line structures[7], and long-delay elements[8]. In Ref.[9], an LWA based on a slow-wave SIW achieved a scanning range of 35° with a fractional bandwidth (FBW) of 3%. Similarly, in Ref.[10], a compact SIW-based LWA incorporating metal vias to induce a slow-wave effect achieved a 50° scan angle within a 7.4% FBW. However, these LP antennas are limited to forward beam scanning because they operate in the fundamental mode of a fast wave. To achieve continuous beam scanning through broadside, the well-known open stopband (OSB) issue must be addressed. Ref.[11] mitigated this by using metal posts to cancel reflections

*Corresponding author, E-mail address: nzynj@nuaa.edu.cn.

How to cite this article: RUAN Yizheng, NIU Zhenyi, CHEN Weikang, et al. Continuous rapid-beam-scanning and circular-polarized leaky-wave antenna based on meandering-SIW with defected ground structures[J]. Transactions of Nanjing University of Aeronautics and Astronautics, 2025, 42(1): 80-89.

http://dx.doi.org/10.16356/j.1005-1120.2025.01.006

from each element, enabling continuous beam scanning from backward to forward across a 60° range within a 9.4% FBW, though the achievable scan angle remains limited. To improve the scanning range, Ref.[12] proposed a double-layer meandering structure that enhances both the scanning rate and the scanning range. In Ref.[13], the impedance matching theory was used to analyze the equivalent circuit model of the unit cell for spoof surface plasmon polaritons (SSPPs) LWAs, with the addition of a capacitive slot to suppress the OSB. In Ref.[14], a sine curve pattern was introduced in the SSPPs transmission line, which shifted the dispersion curve into the fast wave region. However, the antenna gain in this design was limited to no more than 5 dB.

In some cases, circularly polarized (CP) radiation is preferred due to its ability to better suppress rain and fog interference, as well as resist multipath reflections during beam steering. Ref.[15] presented a periodic SIW-based antenna with a wide CP scanning range by adjusting the radiation pattern of two types of slots. Similarly, Ref.[16] discussed a CP LWA based on a CRLH transmission line structure. While these antennas operated over a wide bandwidth, they suffered from a low scanning rate. In Ref.[17], a CP meandering-SIW antenna was proposed. However, the small phase difference between adjacent slots restricted its scanning rate, and the axial ratio (AR) deteriorated as the beam scans from backward to forward. Ref.[18] proposed a millimeter-wave CP continuous transverse stub (CTS) LWA with an improved scanning rate, achieved by alternatively arranging periodic ridges on both plates of a bent parallel plate waveguide (PPW). The CP radiation was generated by a modified metasurface unit based on the Jerusalem cross. However, the antenna's profile height was increased due to the use of CTS arrays for radiation. In Ref.[19], a CP LWA based on a slow-wave SIW structure with a high scanning rate was introduced. The use of asymmetric unit cells eliminated the OSB and achieved a 52° scan angle through broadside. Nevertheless, the circular polarization was achieved by combining two 45° LP antennas through a 3 dB coupler, which complicated the structure. As a result, a more streamlined approach is needed to enhance the scanning rate of CP antennas while maintaining design simplicity and performance efficiency.

In this paper, a high-scanning-rate circular-polarized SIW LWA with continuous beam scanning is proposed. A meandering structure is utilized to minimize the antenna's longitudinal size and improve the scanning rate. Unlike antennas designed by other researchers that employ meandering structures, the proposed design incorporates a ground plane that not only functions as a reflective surface to facilitate electromagnetic wave propagation, but also introduces defected ground structures (DGSs) to enhance overall performance. The DGSs effectively suppress the OSB while maintaining stable CP beams. Furthermore, they contribute to the improved polarization purity at broadside. This integration of meandering structure and DGSs results in a compact and high-performance antenna design, offering continuous CP beam scanning. The proposed LWA is straightforward to fabricate due to its simple feeding mechanism and fully slotted design.

1 Antenna Design and Analysis

1.1 Antenna configuration

The full configuration of the antenna is shown in Fig.1(a). The proposed antenna is designed on the substrate RO4003 with relative permittivity 3.55 and loss tangent of $\tan\delta = 0.002\ 7$. The in-phase superposition of reflected waves at the abrupt right-angle turns leads to impedance mismatching. To address this, metal vias are placed at each turning point of the meandering structure, reducing the input reflection coefficient and enabling more effective wave propagation.

The proposed SIW unit is illustrated in Fig.1(b). The top metal surface features two identical transverse slots and one longitudinal slot, which radiate electromagnetic waves. The bottom layer contains a circular slot, offset by a distance w_p from the center along the x-axis, serving as a DGS. DGSs have played an instrumental role in various applications, including filters, coplanar waveguides, and antennas[20-22]. In this design, they disturb the current flow on the ground plane and contribute to the radiation of electromagnetic energy. The specific parame-

ter values are: dx = 3.5 mm, dy =3.4 mm, l_1 = 7.6 mm, l_2 = 5.2 mm, w_1 = 10 mm, w_2 = 3 mm, w_3 = 2.4 mm, w_4 = 1.2 mm, w_s = 0.4 mm, w_p = 1.68 mm, d = 1.2 mm, s = 2 mm, r_p = 1.8 mm.

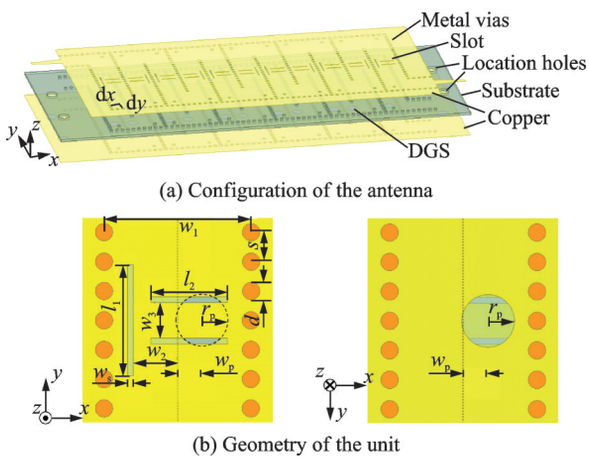

(a) Configuration of the antenna

(b) Geometry of the unit

Fig.1 Antenna structure

1.2 Scanning rate enhancement

The beam scanning rate at the operating frequency f_0 can be described by the partial derivation of $\theta(f)$ with respect to f[23], shown as

$$v_{SR}=\frac{\partial\theta(f_0)}{\partial f}=\frac{1}{k_0\cos\theta(f_0)}\left[\frac{\partial\beta}{\partial f}-\frac{2\pi}{c}\sin\theta(f_0)\right] \tag{1}$$

where k_0 is the free-space wavenumber, β the propagation constant of the leaky mode, and c the speed of light. It indicates that the scanning capability is affected by the rate of change of β with respect to frequency. Once the radiation angle is set, a larger $\partial\beta/\partial f$ leads to a higher scanning rate.

In modern electronic systems, the fractional bandwidth is a more effective measure of spectrum efficiency. Thus, the scanning rate can be defined as the scanning range divided by the FBW. To achieve a high v_{SR}, it is essential to increase the total scanning range. The beam direction can be expressed as

$$\begin{cases}\theta=\arcsin\dfrac{\Delta\varphi}{k_0 p}\\ \Delta\varphi=\beta_{siw}\cdot L\end{cases} \tag{2}$$

where $\Delta\varphi$ is the phase difference, p the period of the structure, L the effective distance between adjacent units, and β_{siw} the propagation constant of the SIW. It implies that the propagation path of the electromagnetic wave can be extended by bending the waveguide. In a conventional SIW, β_{siw} remains constant when the material and operating frequency are fixed. Hence, the increasing L can ultimately enlarge the beam scanning angle, i.e., adopt a meander-line structure.

In general, the main beam direction of a LWA can be approximated as $\theta=\arcsin(\beta/k_0)$. If the structure is meandering and additional transmission lines are incorporated, the beam direction should be calculated as

$$\theta=\arcsin\frac{\beta L'-\pi}{k_0 p} \tag{3}$$

where $\beta L'$ is the total phase shift over the unit cell and π the phase reversal between adjacent units. The total unit length needs to be $n\lambda_g/2$, where n is an odd integer and λ_g the waveguide wavelength. To strike a balance between the antenna size and beam scanning range, n=5 is chosen for this design. Fig.2 illustrates the electric field distribution E of the antenna at a frequency of 11.9 GHz. The five current distribution centers indicate nearly five and a half wavelengths, confirming that $\Delta\varphi$ is 5 times π.

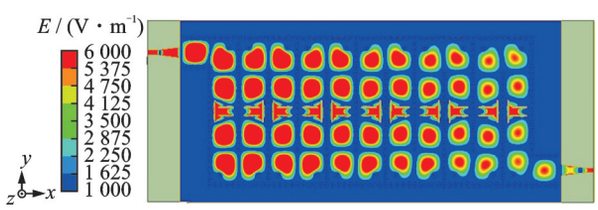

Fig.2 Electrical field distribution of the antenna at 11.9 GHz

1.3 OSB suppression and parametric studies

The reflection coefficient of the antenna, which features only slots on the top plane, is illustrated in Fig.3(a). The curve shows a noticeable bulge, with $|S_{11}|$ rising above −10 dB in the 11.8—12 GHz frequency range. This indicates that the antenna experiences an OSB. In the OSB region, the reflection coefficient degrades, and the antenna gain drops significantly. The increase in reflection within this range is a result of structural mismatch in the design. The simulated ARs of the antenna with only slots on the top plane in the main beam directions also deteriorates within the OSB, as shown in Fig.3(b). To mitigate this issue, offset circular slots are introduced on the ground plane as DGSs. This modification effectively eliminates the OSB in the proposed anten-

na and reduces the AR at broadside. Fig.3(c) compares the gain of antennas with and without DGSs, demonstrating that the former exhibits higher gain. This improvement is attributed to the inevitable disturbance of the fields around the top surface slots caused by the DGSs, leading space harmonics radiating to the upper space across the entire frequency band. The electric field diagrams before and after the loading of DGSs at the OSB frequency of 11.9 GHz are shown in Fig.4. It can be observed that the electric field magnitude on the top radiating slots of antenna with DGSs is stronger than that of the antenna without DGSs. In the antenna without DGSs, as shown in Fig.4(a), the effective radiation is limited to the first few units. In contrast, the antenna with DGSs, as shown in Fig.4(b), generates effective radiation across all units. Furthermore, the suppression of the OSB is supported by the dispersion diagram of the proposed unit cell. Both the attenuation constant α and phase constant β can be calculated using the formulas provided in Ref.[24]. According to Eq.(3), there is a phase reversal between adjacent units in the meandering structure, requiring a revision of the phase constant. The corresponding dispersion diagram, shown in Fig. 5(a), reflects this adjustment. The revised phase shift of zero at a specific frequency indicates normal beam radiation

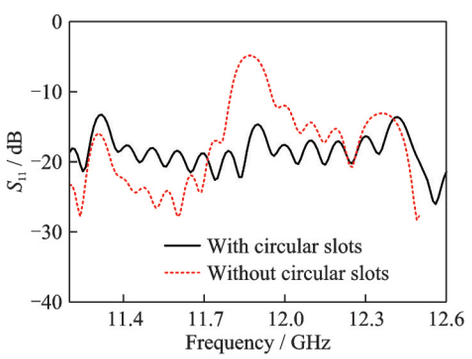

(a) Comparison of simulated reflection coefficients

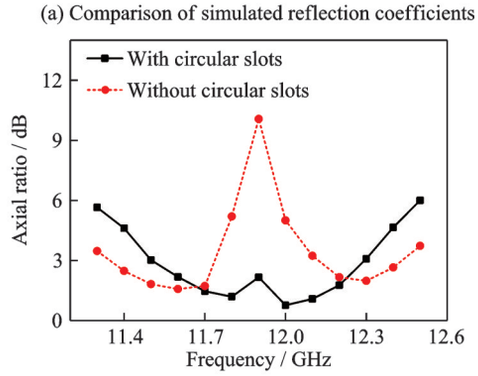

(b) Comparison of simulated AR

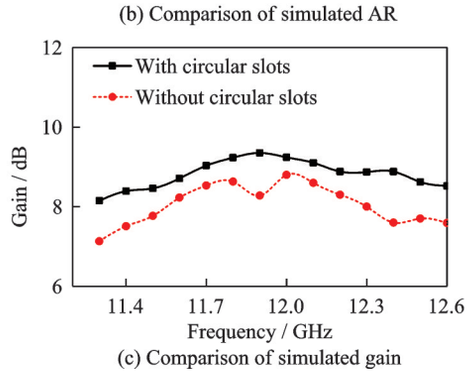

(c) Comparison of simulated gain

Fig.3 Comparison of simulated results for antennas with and without circular slots

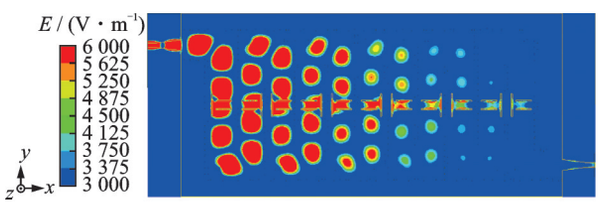

(a) The antenna without DGSs

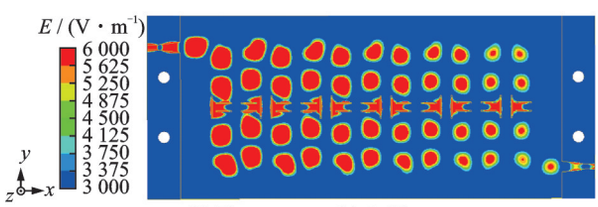

(b) The antenna with DGSs

Fig.4 Electric field distribution of the antenna with different units at the OSB frequency of 11.9 GHz

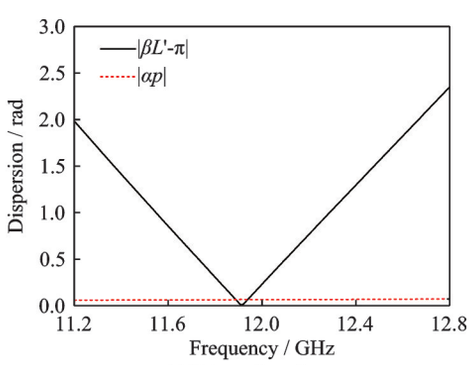

(a) Dispersion diagram

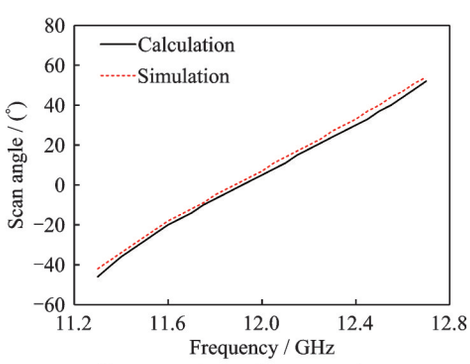

(b) Scan angle for the proposed antenna

Fig.5 Antenna beam scanning performance

at broadside and confirms OSB suppression. Finally, the radiation angle extracted from full-wave simulations aligns closely with the angle calculated from Eq.(3), as depicted in Fig.5(b), further validating the design.

The introduced DGSs must be shown not to compromise the original circular polarization of the antenna. The mechanism of most CP LWAs can be explained from the point of axial asymmetric structure[25]. In this case, the slots on the top plane intersect both transverse and longitudinal currents, successfully generating circular polarization due to the axial asymmetry required for phase quadrature. Fig. 6 displays the surface current distributions on both the top and bottom planes of the antenna at 11.9 GHz. As the phase angle varies from 0 to 360°, the surface current rotates clockwise. This is because the slots on both the upper and lower surfaces produce currents with the same handedness, leading to a combined left-handed CP radiation over the broadside of the antenna. The simulated normalized radiation patterns, shown in Figs.7(a—e), further confirm that the left-handed circular polarization (LHCP) is significantly stronger than the right-handed circular polarization (RHCP). Additionally, the DGSs applied to the LWA lead to power leakage on the ground plane, as indicated by the back lobes in the radiation patterns. This leakage can be mitigated by placing a reflective grid at an appropriate distance behind the antenna. Despite this, the DGSs do not negatively impact the CP radiation performance.

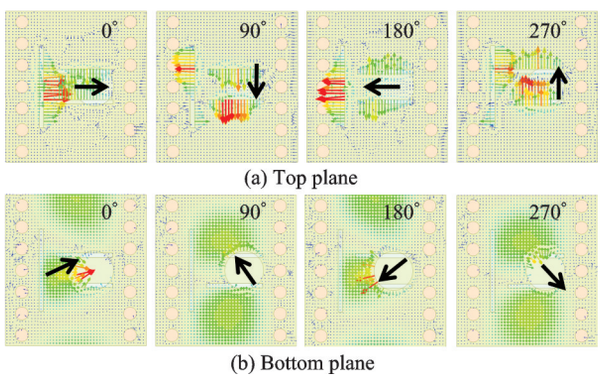

Fig.6 Simulated surface current distribution at 11.9 GHz

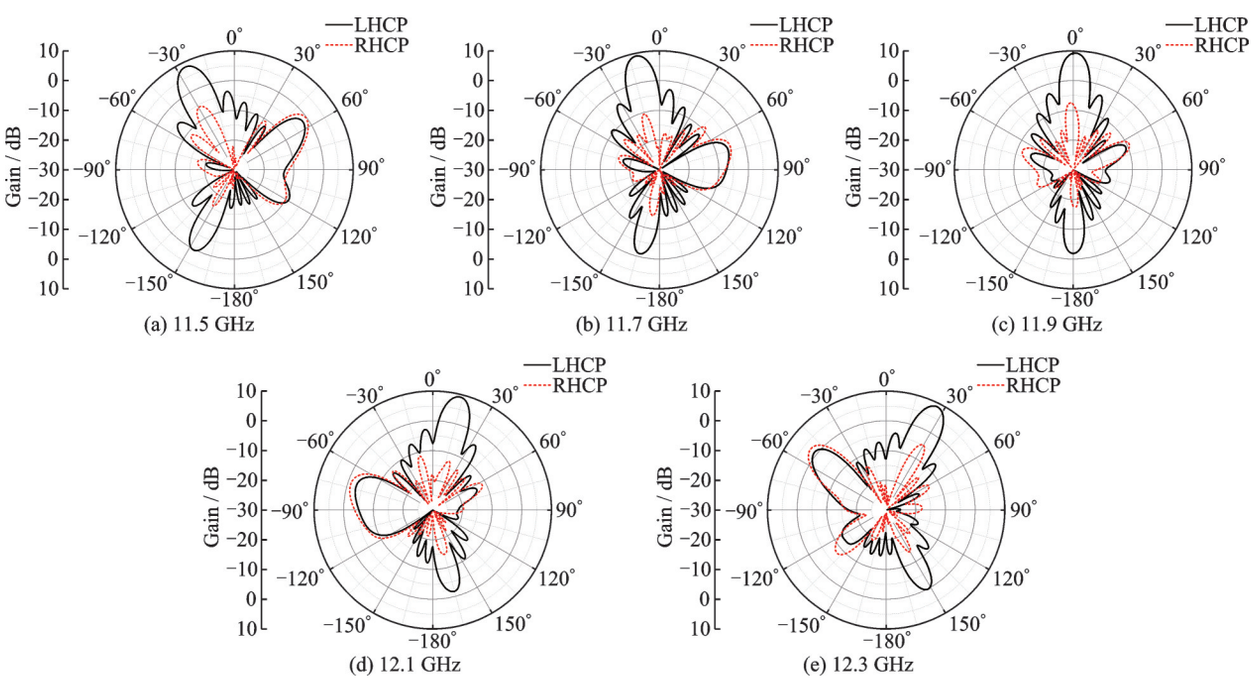

Fig.7 Simulated normalized radiation pattern at different frequencies

A parametric study is conducted to analyze the impact of the circular-shaped DGSs on the S_{11} parameter and AR characteristics in the main beam directions. As shown in Fig.8, the reduction in $|S_{11}|$ within the middle frequency band contributes to the optimization of the AR. When the offset w_p increases gradually from 1.6 mm to 1.8 mm, the AR at the middle frequency rises, while it decreases at both ends of the operating band. In contrast, as the radius r_p increases from 1.7 mm to 1.9 mm, the AR im-

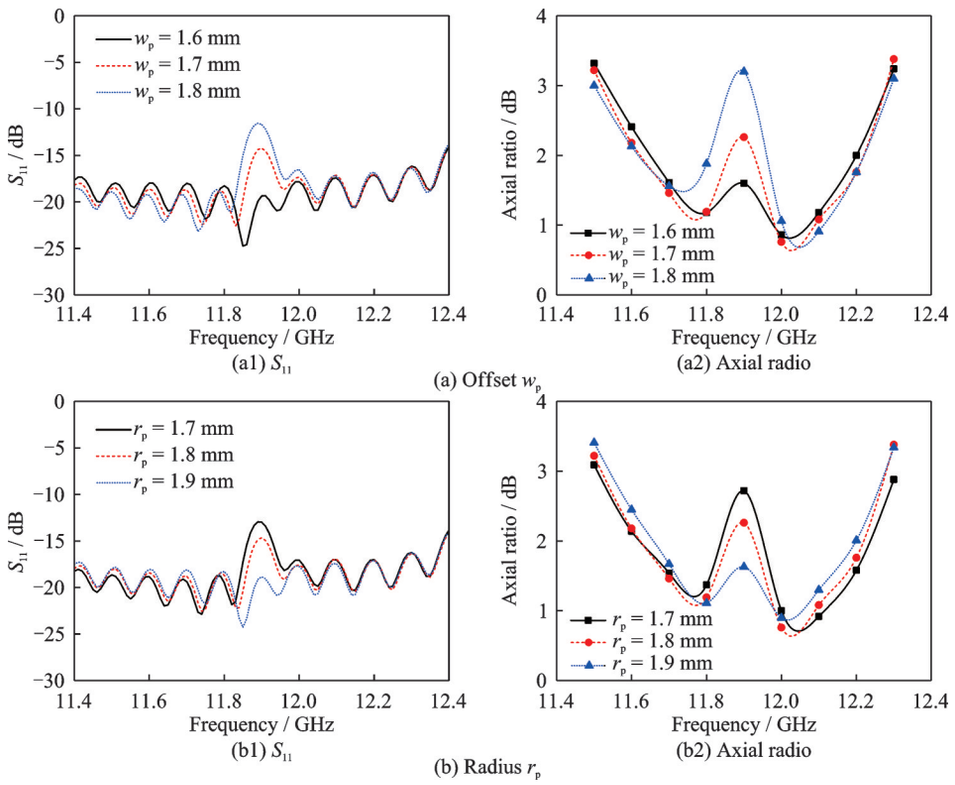

Fig.8 Simulated results of antenna performance as a function of offset w_p and radius r_p

proves at the middle frequency but shows a slight increase at the band edges. Considering practical antenna losses, the final values for w_p and r_p are selected for optimal performance.

2 Experiment and Discussion

The proposed antenna is simulated using ANSOFT HFSS, with a total dimension of 149.2 mm × 61.2 mm × 0.8 mm. A sample of the antenna is designed, fabricated, and measured. The fabricated prototype, produced using standard printed circuit board technology, is shown in Fig.9. The reflection and transmission coefficients are measured by a Keysight N5245A vector network analyzer, and the corresponding results are presented in Fig.10. Overall, the measured and simulated results have similar trends throughout the band. The measured impedance bandwidth ($|S_{11}| < -10$ dB) ranges from 11 GHz to 12.8 GHz, with minor frequency shifts attributed to small fabrication tolerances. The measured $|S_{21}|$ is approximately 5 dB lower than the simulated values, primarily due to connection losses, manufacturing tolerances and measure reflections in the environment.

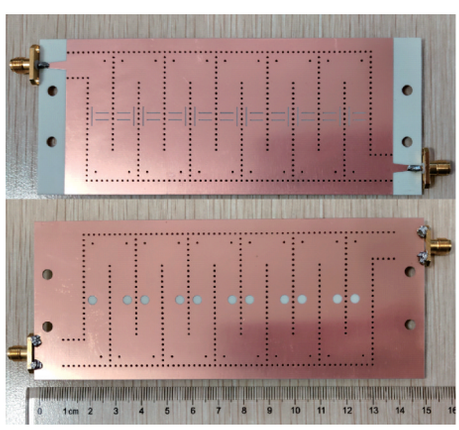

Fig.9 Fabricated prototype

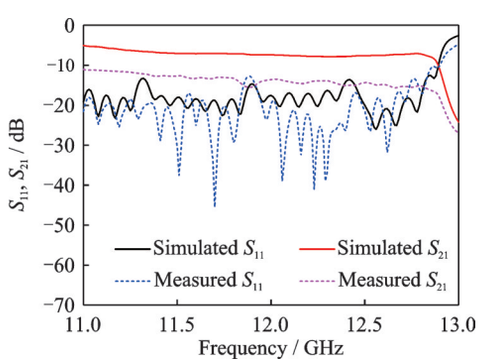

Fig.10 Simulated and measured S_{11}, S_{21}

The far-field radiation patterns are measured in a microwave anechoic chamber, as shown in Fig.11. To minimize the influence of external fac-

tors during measurement, absorbent materials are affixed to both sides of the antenna. The simulated and measured radiation patterns in the xz-plane at eight different frequencies are plotted in Fig.12. While the deviations between the simulated and measured results are within 3°, the overall patterns closely align. The measured main lobe of the 12.7 GHz directional pattern exhibits asymmetry due to partial reflection in the experimental setup when the antenna scans at a large angle. As shown in Fig.12, the DGSs in the antenna induce additional radiation on the ground plane. This effect can be suppressed by placing a reflective grid at an appropriate distance behind the array. The simulated and measured gain and main-beam direction versus frequency are shown in Fig.13. It can be noted that the measured gains are slightly lower than the simulated ones, likely due to material losses and partial absorption of energy by the absorbent materials during large-angle scanning. Despite this, a measured beam-scanning range of 100° is achieved as the frequency varies from 11.3 GHz to 12.7 GHz. As shown in Fig.14, the

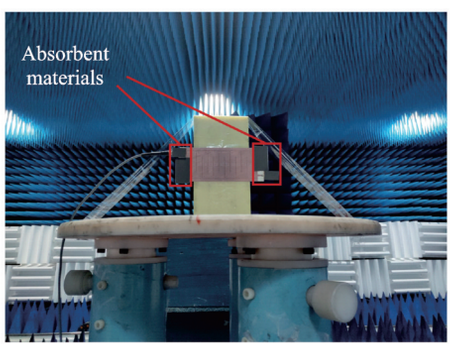

Fig.11 Measurement environment

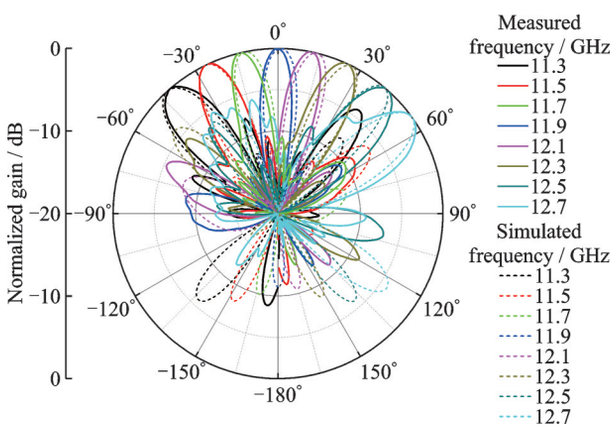

Fig.12 Simulated and measured normalized radiation patterns at different frequencies

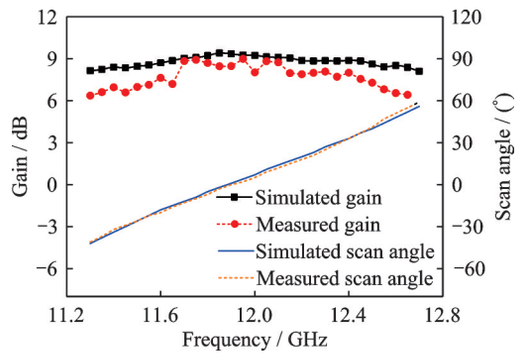

Fig.13 Simulated and measured gain and scan angle at different frequencies

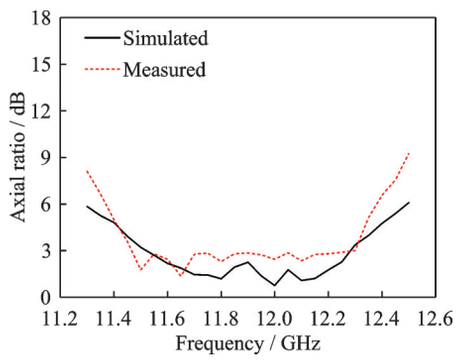

Fig.14 Simulated and measured AR at different frequencies

measured ARs of the main beam directions consistently remain below 3 dB within the 11.5—12.3 GHz range, indicating strong circular polarization performance.

A comparison of key performance parameters between previous works and the proposed antenna is provided in Table 1. While the antennas discussed in Refs.[9-13] achieve a high scanning rate, they exhibit the higher gain variation and are unable to radiate CP waves. In contrast, the antennas from Refs.[16-19] share the same polarization characteristics as the proposed design but face other limitations. Specifically, the antennas in Refs.[16-17] require additional bandwidth to cover scanning range, as reflected in their FBW, which results in a reduced scanning rate. Additionally, the antenna in Ref.[18], composed of a PPW-based CTS array, a power divider-based linear source generator, and a linear-to-circular metasurface polarizer, achieves a high scanning rate but results in an increased overall profile. Similarly, the antenna in Ref.[19], which integrates two slow-wave LP antennas to achieve both circular polarization and a high scanning rate,

Table 1 Comparison of performance with different references

Reference	Implementation method	Center frequency/GHz	FBW/%	Size	Scanning range/(°)	Polarization	SR	Gain variation /dB
[9]	Slow-wave SIW	13.7	3	$8.68\lambda_0\times0.91\lambda_0\times0.02\lambda_0$	35(2—37)	LP	11.7	4.1
[10]	Slow-wave SIW	8.1	7.4	$8.11\lambda_0\times1.08\lambda_0\times0.03\lambda_0$	50(15—65)	LP	6.7	7.0
[11]	Meandering SIW	25.45	9.4	N/A	60(−30—30)	LP	6.4	3.5
[12]	DL-Meandering SIW	13.15	6.5	$4.0\lambda_0\times3.6\lambda_0\times0.04\lambda_0$	107(−58—49)	LP	16.5	4.7
[13]	Microstrip SSPPs	9.45	15.9	$7.37\lambda_0\times0.79\lambda_0\times0.05\lambda_0$	140(−72—68)	LP	8.8	5.5
[16]	CRLH SIW	9.1	33.0	$3.61\lambda_0\times0.57\lambda_0\times0.05\lambda_0$	109(−38—71)	CP	3.3	2.4
[17]	Meandering SIW	16	18.8	$4.27\lambda_0\times1.71\lambda_0\times0.03\lambda_0$	69(−47—22)	CP	3.7	4.5
[18]	PPW+Metasurface	30.05	11.6	$8.22\lambda_0\times6.01\lambda_0\times3.5\lambda_0$	108(−56—52)	CP	9.3	3.8
[19]	Slow-wave SIW	10.3	9.7	$11.43\lambda_0\times1.37\lambda_0\times0.02\lambda_0$	52(−30—22)	CP	5.4	4.0
This work	Meandering SIW	12	11.7	$5.97\lambda_0\times2.45\lambda_0\times0.03\lambda_0$	100(−41—59)	CP	8.6	2.5

DL:Double-layer; N/A:Not available; SR: Scanning rate.

introduces additional structural complexity. In contrast, the proposed LWA has a simpler and low-profile design with a high scanning rate over a wide scanning range, relatively low gain variation, and enables seamless beam scanning from backward to forward.

3 Conclusions

A compact, high-scanning-rate, circular-polarized meandering-SIW LWA with continuous beam scanning is proposed. The challenge of achieving circular polarization using only upper surface slots in the meandering structure is analyzed across the operating band. By embedding circular DGSs periodically on the ground plane, the OSB is effectively suppressed, and the circular polarization purity at broadside is enhanced. The proposed antenna achieves a high scanning rate of 8.6, with a wide scan angle from −41° to 59° within the 11.3—12.7 GHz operating band, while maintaining strong circular polarization between 11.5 GHz and 12.3 GHz. This antenna, with its rapid beam scanning capability, is well-suited for narrow-band wireless communication systems that require circular polarization.

References

[1] JACKSON D R, OLINER A A. Modern antenna handbook[M]. New York, NY, USA: Wiley, 2008.

[2] JACKSON D R, CALOZ C, ITOH T. Leaky-wave antennas[J]. Proceedings of IEEE, 2012, 100(7): 2194-2206.

[3] WEI D, LI J, YANG J, et al. Wide-scanning-angle leaky-wave array antenna based on microstrip SSPPs-TL[J]. IEEE Antennas Wireless Propagation Letters, 2018, 17(8): 1566-1570.

[4] ZHANG Y, LIU H, MENG C, et al. A novel millimeter-wave backward to forward scanning periodic leaky-wave antenna based on two different radiator types[J]. Progress in Electromagnetics Research, 2020, 168: 31-38.

[5] JIDI L, CAO X, GAO J, et al. Ultrawide-angle and high-scanning-rate leaky wave antenna based on spoof surface plasmon polaritons[J]. IEEE Transactions on Antennas and Propagation, 2022, 70(3): 2312-2317.

[6] ZHANG H H, LI R, REN J, et al. High-scanning-rate and wide-scanning-angle leaky-wave antenna based on double-layer slow-wave structure[J]. IEEE Antennas and Wireless Propagation Letters, 2023, 22(9): 2145-2149.

[7] YANG W, PENG Z, REN J, et al. Composite right/left-handed leaky-wave antenna with high scanning rate[J]. IEEE Antennas and Wireless Propagation Letters, 2022, 21(12): 2522-2526.

[8] MACKAY A J, ELEFTHERIADES G V. Meandered and dispersion-enhanced planar leaky-wave antenna with fast beam scanning[J]. IEEE Antennas and Wireless Propagation Letters, 2021, 20(8): 1596-1600.

[9] GUAN D F, ZHANG Q, YOU P, et al. Scanning rate enhancement of leaky-wave antennas using slow-wave substrate integrated waveguide structure[J]. IEEE Transactions on Antennas and Propagation, 2018, 66(7): 3747-3751.

[10] KHALIL M, KAMAREI M, JOMAAH J, et al. Compact SIW leaky wave antenna[C]//Proceedings of the Third International Conference on Technological Advances in Electrical, Electronics and Computer Engineering (TAEECE). Beirut, Lebanon: IEEE, 2015: 124-129.

[11] CAO W, HONG W, CHEN Z N, et al. Gain enhancement of beam scanning substrate integrated waveguide slot array antennas using a phase-correcting grating cover[J]. IEEE Transactions on Antennas and Propagation, 2014, 62(9): 4584-4591.

[12] LUO P, HE W, ZHANG Y, et al. Leaky-wave antenna with wide scanning range based on double-layer substrate integrated waveguide[J]. IEEE Access, 2020, 8: 199899-199908.

[13] LEI S, WEI G, HAN K, et al. Wide-range leaky-wave antenna with high scanning rate and OSB suppression[J]. AEU International Journal of Electronics and Communications, 2023, 168: 154705.

[14] WANG Y, LIU S Y, GUAN C S, et al. Linearly scanning spoof surface plasmon polaritons leaky-wave antenna with high scanning rate[J]. IEEE Open Journal of Antennas and Propagation, 2024, 5(1): 153-163.

[15] LYU Y L, MENG F Y, YANG G H, et al. Periodic SIW leaky-wave antenna with large circularly polarized beam scanning range[J]. IEEE Antennas Wireless Propagation Letters, 2017, 16: 2493-2496.

[16] AGARWAL R, YADAVA R L, DAS S. A multilayered SIW-based circularly polarized CRLH leaky wave antenna[J]. IEEE Transactions on Antennas and Propagation, 2021, 69(10): 6312-6321.

[17] LI B, ZHONG H, MA W, et al. A circularly polarized substrate integrated waveguide slot array antenna with enhanced scanning range[C]//Proceedings of the 2019 International Conference on Microwave and Millimeter Wave Technology (ICMMT). Guangzhou, China: IEEE, 2019: 1-3.

[18] CAO Q D, YANG X X, YU F, et al. High scanning rate millimeter-wave circularly polarized CTS leaky wave antenna[J]. IEEE Transactions on Antennas and Propagation, 2024, 72(7): 6087-6092.

[19] ZHONG J, RASHID A K, ZHANG Q. 45° linearly polarized and circularly polarized high-scanning-rate leaky-wave antennas based on slotted substrate integrated waveguide[J]. IEEE Access, 2020, 8: 82162-82172.

[20] WEI K, LI J, WANG L, et al. Mutual coupling reduction by novel fractal defected ground structure bandgap filter[J]. IEEE Transactions on Antennas and Propagation, 2016, 64(10): 4328-4335.

[21] WANG J, NING H, MAO L. A compact reconfigurable bandstop resonator using defected ground structure on coplanar waveguide[J]. IEEE Antennas and Wireless Propagation Letters, 2012, 11: 457-459.

[22] GAO D, CAO Z X, FU S D, et al. A novel slot-array defected ground structure for decoupling microstrip antenna array[J]. IEEE Transactions on Antennas and Propagation, 2020, 68(10): 7027-7038.

[23] CHEN J, YUAN W, TANG W X, et al. Linearly sweeping leaky-wave antenna with high scanning rate [J]. IEEE Transactions on Antennas and Propagation, 2021, 69(6): 3214-3223.

[24] LYU Y L, LIU X X, WANG P Y, et al. Leaky-wave antennas based on noncutoff substrate integrated waveguide supporting beam scanning from backward to forward[J]. IEEE Transactions on Antennas and Propagation, 2016, 64(6): 2155-2164.

[25] OTTO S, CHEN Z, AL-BASSAM A, et al. Circular polarization of periodic leaky-wave antennas with axial asymmetry: Theoretical proof and experimental demonstration[J]. IEEE Transactions on Antennas and Propagation, 2014, 62(4): 1817-1829.

Authors

The first author Mr. **RUAN Yizheng** received the B.S. degree in electronic and information engineering from Nanjing University of Aeronautics and Astronautics (NUAA), Nanjing, China, in 2018. He is currently pursuing the Ph.D. degree in communication and information system at NUAA, Nanjing, China. His research is focused on metamaterial and antenna theory, and machine learning-based electromagnetic parametric modeling and optimization.

The corresponding author Dr. **NIU Zhenyi** received the BS. degree in electronic engineering and M.E. degree in electromagnetic field and microwave technology from NUAA, Nanjing, China, in 1997 and 2000, respectively, and the Ph.D. degree in radio engineering from State Key Laboratory of Millimeter Waves, Southeast University, Nanjing, China, in 2006. He is currently an associate professor with College of Electronic and Information Engineering, NUAA. His research interests include computational electromagnetics, antenna design, and electromagnetic compatibility.

Author contributions Mr. **RUAN Yizheng** designed the study, complied the models, conducted the analysis, interpreted the results, and wrote the manuscript. Dr. **NIU Zhenyi** contributed to the discussion and manuscript

revision. Mr. **CHEN Weikang** contributed to the result interpretation and experiment analysis. Prof. **ZHAO Yongjiu** contributed to the discussion and revision of the study. Prof. **PAN Shilong** contributed to the discussion and background of the study. All authors commented on the manuscript draft and approved the submission.

Competing interests The authors declare no competing interests.

(Production Editor: SUN Jing)

基于曲折SIW与缺陷地结构的连续快速波束扫描圆极化漏波天线

阮一铮，牛臻弋，陈伟康，赵永久，潘时龙

(南京航空航天大学微波光子技术国家级重点实验室，南京 211106，中国)

摘要：提出了一种基于曲折基片集成波导(Substrate integrated waveguide, SIW)和缺陷地结构(Defected ground structures, DGSs)的紧凑型高扫描速率圆极化漏波天线(Leaky-wave antenna, LWA)。该设计通过引入曲折形SIW结构提升波束扫描速率，并利用顶部金属层刻蚀的π形缝隙实现圆极化辐射。为有效抑制宽边辐射时的开阻带效应，在地平面周期性刻蚀偏置圆形DGSs单元，并通过参数化研究系统揭示了缺陷地结构对天线反射系数和轴比特性的调控机制。最后对天线原型进行仿真、加工及测试，结果表明：在11.3～12.7 GHz工作频段内，波束可实现－41°至59°的连续扫描，扫描速率达到8.6；在11.5～12.3 GHz频段内天线轴比保持在3 dB以下。该设计在频谱资源日益受限的无线通信系统中展现出显著应用价值。

关键词：漏波天线；扫描速率；圆极化；开阻带；缺陷地结构